An insight into drying-wetting cycles of peat

Luis J. Parra-Gómez[1*], *Stefano* Muraro[1], and *Cristina* Jommi[1,2]

[1] Delft University of Technology, Faculty of Civil Engineering and Geosciences, 2628CN Delft, The Netherlands
[2] Politecnico di Milano, School of Civil, Environmental and Land Management Engineering, 20133 Milano, Italy

Abstract. A relevant part of the geotechnical infrastructure in the north of Europe and overseas is built on soft organic soils, including peat. Peat is extremely vulnerable to climate-related hazards as increased temperature accelerates drying, shrinkage and decomposition of the organic matter. Peat exhibits dramatic changes in volume with changes in water content. As the material deforms, the pore space evolves and changes the water retention response. The evolution of the pore space leads to a hysteretic relationship between suction, water content, and void size distribution. In this work, data from free shrinkage-swelling and suction measurements on natural fibrous peat subjected to drying and wetting cycles are presented and discussed. The water retention and shrinkage behaviour of the samples are modelled by accounting for capillarity and considering the evolution of the pore size distribution. X-Ray computer tomography was used to explore the change in the pore space upon shrinkage and drying. The experimental evidence shows that peat experiences distinct shrinkage zones including one where accelerated contraction occurs. Such behaviour is explained as a consequence of the interactions of an aggregated fabric. This is supported by the conceptual modelling approach that highlights the pivotal role of the evolving pore space.

1 Introduction

Peatland areas are estimated to cover 2.84% of the global land area, amounting to 4.23 million km^2 spread across all continents [1]. All across the world, infrastructure projects are developed over peat deposits or use peat as construction material. This is the case in the Netherlands, where 3500 km of regional dykes are made of peat and play a crucial role in ensuring the safety of a significant portion of the country [2].

The projected rise in average global temperatures expected during the XXI century will affect infrastructure built in peatland areas. Temperature fluctuations are expected to increase the magnitude and frequency of extreme rainfall and drought events, causing unprecedented wetting and drying cycles in the peat deposits. This will cause problems for peat-based infrastructure arising from cyclic shrinkage and swelling, superficial and internal cracking, internal erosion, and degradation [3]. These effects impact the safety and serviceability of existing infrastructure but also increase greenhouse gas emissions by releasing the carbon sequestered within the organic matter.

From the soil mechanics perspective, peat is a non-conventional soil. It has very high porosity, usually above 90%, high organic content, very large compressibility and, simultaneously, high friction angles due to the reinforcing effects of fibres. The material often experiences large volumetric strains upon loading or drying, which cause dramatic fabric changes throughout any mechanical or hydraulic process [4]. This evolution of the fabric leads to severe changes in the material response, such as the hydraulic conductivity, which has been reported to decrease by several orders of magnitude upon compression [5]. In this work, experimental evidence regarding wetting and drying cycles in peat is presented. Experimental data is accompanied by a simple conceptual model to understand the evolution of shrinkage and water retention as a consequence of the changes in the pore size distribution of the material.

2 Experimental evidence

A simple experimental test was set up to investigate the drying process in natural fibrous peat. Samples recovered from the Leendert de Boerspolder site in the Netherlands were collected and subjected to drying and wetting. The material consists of peat recovered from the polder of the dyke at a depth of 2.5 m below the ground surface, which has an average initial void ratio, e_0 = 10.5, specific gravity, G_s = 1.504 determined with a gas pycnometer, organic content OC = 58% and fibre content FC = 17% [6]–[8].

Two specimens were prepared and subjected to drying and wetting cycles in a temperature-controlled room with a temperature of 20.5°C ± 0.5° and a relative humidity of 36% ± 6%.

The first specimen was carved into a cylinder with a diameter of 8 cm and equal height and dried while monitoring the development of suction and its weight in a Hyprop 2 (HYP) equipment [9]. Height and diameter measurements were regularly taken during the test using a digital calliper with an accuracy of 0.01 mm and taking

* Corresponding author: L.J.ParraGomez@tudelft.nl

care to minimise sample disturbance. Three drying (DC) and two wetting cycles (DW) were performed during the test. Initially, the sample was saturated by capillary rise and placed on the equipment. Once the pressure readings stabilised, the sample was uncovered and allowed to dry in stages, covering it at regular intervals to allow for water content homogenisation. Once the sample reached an average suction of about 50 kPa, the sample was wetted from the top and covered in stages. Once suction reached values close to zero, the process was repeated, letting the suction increase to an average value of about 85 kPa. Finally, the sample was dried in stages until the top and bottom measuring shafts cavitated. After cavitation, two sub-samples were recovered close to the sensing points and used to measure further suction development in a WP4C potentiometer.

Due to the process needed to dismount the sample from the Hyprop, volume measurements had to stop after the maximum cavitation pressure. Thus, a second specimen, FS, was carved into a 4.6 cm diameter cylinder with the same height, and it was dried while keeping track of its weight. To improve the volume measurement accuracy while accommodating the large displacements and distortions that the sample suffers at high suction ranges, the volume of the second specimen was tracked using a system of laser distance sensors. A three-laser setup was used to reconstruct radial profiles of the sample in twelve angular directions. The data was processed to define a point cloud and operated to calculate the volume and strains of the sample.

Fig. 1 shows the shrinkage curve in terms of void ratio, e, and water ratio, e_w, for both specimens. Good agreement is found between both samples and measuring techniques. The literature describes four characteristic shrinkage zones for mineral materials: proportional, structural, residual and zero shrinkage [10]. The drying process in the measured sample starts with a small amount of proportional or normal shrinkage at water ratios greater than 10.0 (degree of saturation, $S_r \cong 0.95$). During proportional shrinkage, the loss in water volume is similar to the reduction in the void volume with a slope of the curve close to 1.0. Between water ratios of 10.0 and 8.5 ($S_r \cong 0.86$), the curve displays structural shrinkage, characterised by a loss of water volume higher than the loss in volume of the sample and a slope smaller than 1.0. Following the structural shrinkage, the curve displays a second large zone of proportional shrinkage between water ratios of 8.5 and 3.0 ($S_r \cong 0.67$). At this point, the shrinkage curve does not show residual shrinkage as commonly found in mineral soils. Between water ratios of 3.0 and 0.6 ($S_r \cong 0.41$), the volume change of the sample is larger than the volume of water loss with a slope higher than 1.0. This shrinkage acceleration has been previously observed in highly organic soils [11], [12]. Finally, although seldom reported in the literature, at water ratios below 0.6, the sample eventually exhibits residual shrinkage and asymptotically approaches zero shrinkage. In all figures, the dashed lines denote the water ratio at the transition between zones.

Fig. 2 presents the corresponding water retention domain, which evolves as the sample contracts during drying. Upon wetting, the scanning curves arrive at different void ratios due to the permanent volumetric strain accumulated during drying. A small hysteresis is also observed during the wetting and re-drying cycles.

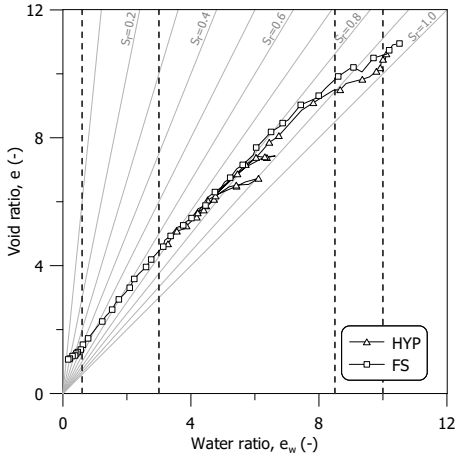

Fig. 1. Shrinkage curve measured for both specimens.

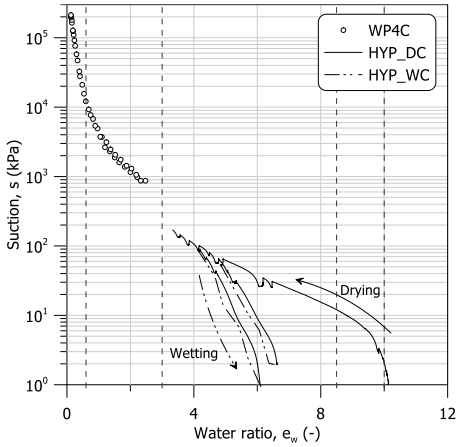

Fig. 2. Water retention domain for the tested material.

The wetting-drying response shows a transition once the previously experienced suction level is reached. This can be better observed in Fig. 3, where the void ratio evolution is shown with respect to the average skeleton stress, $\hat{p}$, defined as:

$$\hat{p} = p - u_f = p - u_{atm} + S_r(u_{atm} - u_w) \qquad (1)$$

where p is the mean total stress, u_{atm} is the atmospheric pressure, and $u_{atm} - u_w$ is the measured suction, s. The void ratio and suction exhibit an approximately bilinear relationship in logarithmic space akin to the over-consolidated to normally consolidated transition described for mechanical loading [13], [14].

The laser measurements provide insight into the deformation mode of the sample upon drying during the shrinkage test. Fig. 4 shows the evolution of the strain ratio between the radial, ε_r, and axial strain, ε_a. The plot shows an initial anisotropic shrinkage with predominant radial strain. The shrinkage approaches the isotropic condition at a water ratio of about 5.0. Recently, a similar response was described by Zhao, who suggested that it could be related to anisotropic inter-aggregate porosity and mostly isotropic shrinkage of intra-aggregate voids, which are engaged at a lower water ratio [4]. The experimental data suggest that to completely describe the contraction experienced during

drying, it is essential to expand the view to the evolution of the pore size distribution beyond the pore volume change.

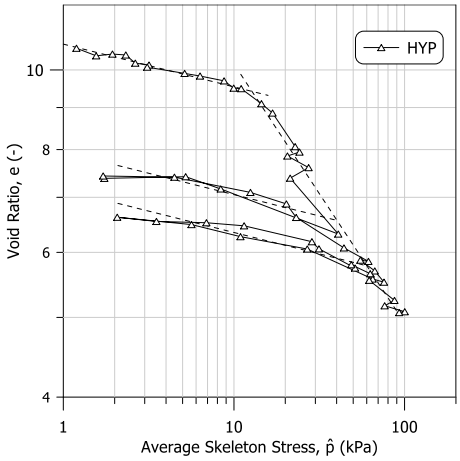

Fig. 3. Variation in void ratio with the average skeleton stress during drying and wetting.

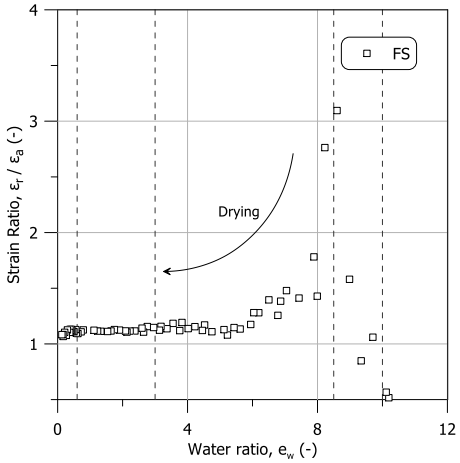

Fig. 4. Evolution of radial to axial strain ratio with water ratio.

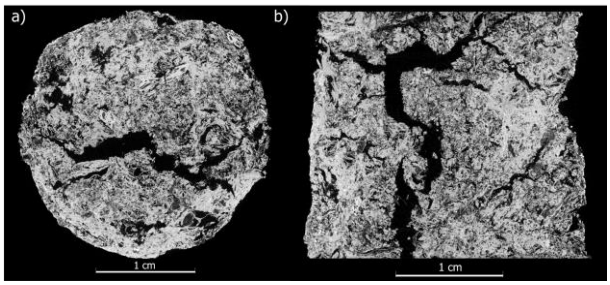

Fig. 5. Internal structure observed in the CT Scan. a) Top view at the middle of the sample; b) Frontal cross-section.

After drying, sample FS was scanned in an X-Ray computer tomography apparatus to observe its internal structure. Horizontal and vertical cross-sections of the sample are shown in Fig. 5. The scan shows that the dry sample contains large voids between aggregations or peds of finer material, which contract towards different centres of mass. These large voids develop mainly internally and are not necessarily visible from the sample's boundary. These voids are likely caused by differential shrinkage of different peds upon drying, and they may suffer non-homothetic contraction response as already observed on clays [15], supporting those interpretations based on inter- and intra-aggregates porosities [16], [17]. The images taken at very dry conditions suggest that macro voids can still be generated at a low void ratio.

3 A simple conceptual framework

3.1 Model formulation

The experimental evidence shows that the deformation mechanism in peat under drying goes through multiple phases characterised by the interplay between the amount of water volume lost and the change in the sample volume. Considering that peat is unique due to its extremely high porosity, a simple conceptual framework is proposed to gather insight into the nature of peat shrinkage and retention behaviour based on the evolution of its pore size distribution. Let $f^e(\phi, \hat{p})$ be a function representing the distribution of the volume of pores of characteristic size (ϕ) normalised by the volume of solids at a given average skeleton stress, $\hat{p}$. The void ratio, e, can be obtained as:

$$e(\hat{p}) = \int_0^\infty f^e(\phi, \hat{p})\ d\phi \tag{2}$$

The function $f^e(\phi, \hat{p})$ is related to the commonly used pore size distribution function $\mathrm{PSD}(\phi, \hat{p})$ and the relative frequency of pore sizes $f(\phi, \hat{p})$ by Equation 3.

$$f^e(\phi, \hat{p}) = e \cdot f(\phi, \hat{p}) = \frac{\mathrm{PSD}(\phi, \hat{p})}{\ln(10) \cdot \phi} \tag{3}$$

The function $f^e(\phi, \hat{p})$ is usually inferred from experimental techniques such as mercury intrusion porosimetry (MIP), notwithstanding the known limitations caused by the sequential intrusion of the pore space. A theoretical distribution will be used in the following to support the conceptual development.

The air entry value of a given pore size, $\psi_{AE}(\phi)$, can be estimated using the Young-Laplace equation:

$$\psi_{AE}(\phi) = \frac{2T\cos\theta}{\phi} \tag{4}$$

where T is the fluid surface tension, and θ is the contact angle between the fluid and the solid particles. Note that θ can vary during the drying process as the organic matter can lose affinity for water and even become hydrophobic when exposed to oxygen. Under the assumptions of the capillary bundle model, the Young Laplace equation provides a way of evaluating the saturation of each pore size in the soil at a given suction level, s, according to Equation 5. This assumption disregards pore network connectivity.

$$S_r(\phi, s) = \begin{cases} 1, & \text{for } s \le \psi_{AE}(\phi) \\ S_{r,res} & \text{for } s > \psi_{AE}(\phi) \end{cases} \tag{5}$$

where $S_{r,res}$ represents a residual saturation inside the pore after air entry is reached. The residual saturation can be taken as zero or as a constant to account for the water retained through adsorption.

The compressibility of the peat sample is described by a bilinear relation in the logarithm of void ratio and average skeleton stress, as shown by the experimental

evidence in Fig. 3. The average skeleton stress of a soil sample under free drying is simply $S_r s$. The bilinear relationship of the overall sample volume change is assumed to be valid at all scales of the void ratio distributions. Under this assumption, the evolution law for the void ratio distribution with respect to the average skeleton stress reads as:

$$f^e(\phi,\hat{p}) = \begin{cases} f^e(\phi,\hat{p}_0)\dfrac{\hat{p}_0^{\kappa^*}}{p^{\kappa^*}} & \text{for } \hat{p} \le \hat{p}_p \\ f^e(\phi,\hat{p}_0)\dfrac{\hat{p}_0^{\lambda^*}\hat{p}_p^{(\lambda^*-\kappa^*)}}{\hat{p}^{\lambda^*}} & \text{for } \hat{p} > \hat{p}_p \end{cases} \quad (6)$$

where $f^e(\phi,\hat{p}_0)$ denotes the initial void ratio distribution taken at the reference stress level $\hat{p}_0$ (equal to 1 kPa), $\hat{p}_p$ is the observed pre-consolidation stress, and λ^* and κ^* are the loading and unloading-reloading coefficients. This hypothesis on the compression behaviour implies that volume change originates only in the rearrangement of the position of solids whose volume remains constant throughout the process. The proposed compressibility relationship for the evolution of the pore space is a reasonable assumption under the capillary bundle model, as each pore class remains saturated until suction exceeds its air entry value. The parameters λ^* and κ^* are average values which, overall, comply with the volumetric response of the sample, such as the one shown in Fig. 3, although they could vary with the pore size across scales. For the sake of simplicity in this work, λ^* and κ^* are assumed constant. Under the above-mentioned hypotheses, the average skeleton stress acting on each pore class can be written as:

$$\hat{p} = \begin{cases} s & \text{for } s \le \psi_{AE}(\phi) \\ \psi_{AE}(\phi) & \text{for } s > \psi_{AE}(\phi) \end{cases} \quad (7)$$

With equations 6 and 7, the reduction in pore volume density can be calculated for each pore class. However, a reduction in the volume is accompanied by a change in pore size that must be considered. Using a logarithmic strain definition, the change in size expected from the linear strain can be calculated by:

$$\phi = \phi_0 \left(\frac{f^e(\phi,\hat{p})}{f^e(\phi,\hat{p}_0)} \right)^{\alpha} \quad (8)$$

where ϕ_0 is the initial size of the pore class and α is a coefficient equal to one-third under isotropic conditions. Equations 6 to 8 provide the means to describe the evolution of the void ratio distribution at increasing suction levels. Note that the suction is assumed to be constant irrespective of the pore size. Therefore an equalised suction distribution is assumed. For a given suction, the overall void ratio, degree of saturation and water ratio can be calculated by integration as:

$$e = \int_0^{\infty} f^e(\phi,\hat{p})\, d\phi \quad (9)$$

$$S_r = \frac{1}{e}\int_0^{\infty} f^e(\phi,\hat{p}) \cdot S_r(\phi,s)\, d\phi \quad (10)$$

$$e_w = eS_r \quad (11)$$

3.2 Model performance

The model performance is demonstrated for different pore size distributions and parameters. First, as a baseline, the model is applied to a pore size distribution expected for a clay. Distribution 1 represents a unimodal distribution of pores around 0.1 μm similar to that described by [18], and it is modelled with $e_0 = 1.0$, $G_s = 2.65$, $\lambda^* = 0.20$, $\kappa^* = 0.02$ and $\hat{p}_p = 10$ kPa.

Fig. 6 shows that the predicted water retention and shrinkage curves are consistent with the expected behaviour. The shrinkage curve shows proportional shrinkage followed by residual and zero shrinkage. The influence of the pre-consolidation pressure can be observed in the water retention (SWR) with a sharp change in slope at 10 kPa. The evolution of the pore size distribution shows that both the pore volume and size decrease with increasing suction. However, once suction causes the desaturation of a given pore class, its volume density freezes at the corresponding air entry value. This mechanism replicates the transition to zero shrinkage.

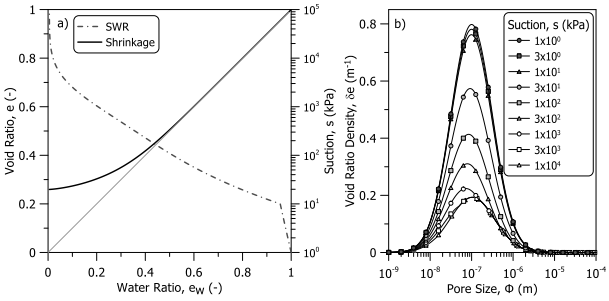

Fig. 6. Model predictions for Distribution 1; a) shrinkage and soil water retention curves; b) evolution of the pore size distribution.

Information on the pore size distribution for peat samples is very scarce, largely due to the difficulty of performing MIP on such soft soil, with the exception of [19]. Two theoretical distributions are explored in an attempt to offer insight into the experimental results previously described. Distribution 2 represents a bimodal pore structure as the one often recalled to describe the fabric of peat. The pore space is represented by a macropore network with an average size of 20 μm, which includes the inter-aggregate pores (Fig. 7c). This is accompanied by a second mode of pores with a mean size of 0.02 μm that spreads across a broader range of sizes and represents the intra-aggregate porosity. Distribution 3 is inspired by the pore size distribution reported by Yamaguchi [19] (Fig. 7d). Both distributions evolve according to the parameters determined for the tested peat: $e_0 = 10.5$, $G_s = 1.505$, $\lambda^* = 0.315$, $\kappa^* = 0.052$ and $\hat{p}_p = 15$ kPa. Fig. 7 shows the model performance compared to the experimental data.

In both cases, the model can capture the evolution of the structural shrinkage and its transition into a proportional zone. Distribution 2 shows a satisfactory agreement with the experimental data up to a water ratio of 3.0, which marks the start of accelerating shrinkage (Fig. 7a). On the contrary, for lower water ratios, the model predicts a residual shrinkage and eventually a higher final void ratio than the one attained by the samples. The agreement on the retention curve is less

satisfactory, with the model showing faster desaturation at increasing suction (Fig. 7b).

Distribution 3 underestimates the void ratio during shrinkage up to a water ratio of 3.0. The difference between the model predictions of the structural shrinkage comes from the different amounts of macro-pores that dry and get frozen faster in distribution 2 than in distribution 3 (Fig. 7c and 7d). The latter shows better agreement with the soil water retention data at suctions lower than 50 kPa but performs similarly to distribution 2 at higher values.

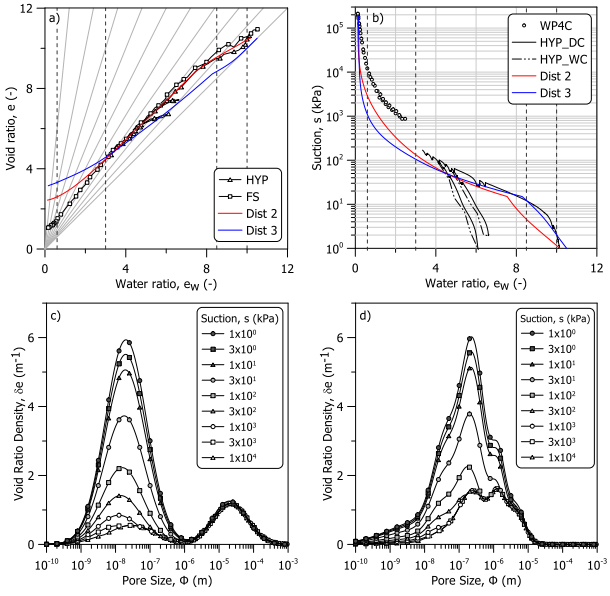

Fig. 7. Model predictions for Distributions 2 and 3; a) shrinkage; b) soil water retention; c) pore size evolution (Distribution 2); d) pore size evolution (Distribution 3)

4 Discussion

The previous description of the evolution of the pore size distribution is a tantalising option to explain the features of drying in peat. The model is able to capture the differential effects that occur in different pore sizes or classes, which results in predicted responses that agree with commonly observed shrinkage patterns.

Nonetheless, various assumptions were introduced in the model construction, which limits its predictive capability. It assumes that shrinkage is compliant across scales, in turn linking all deformation of the pore space to the overall volume change of the sample. This implies that the evolution of the pore space can only shrink existing pores and cannot generate new voids through differential processes like multiscale drying [17].

The model fails to predict the accelerated shrinkage response observed in the tested peat starting from a water ratio of 3.0. One of the possible explanations for this behaviour comes from differential drying of the different pore classes, as schematically illustrated in Fig. 8. Fig. 8a illustrates proportional shrinkage occurring under constant saturation (stage 1). This is followed by Fig. 8b, which shows the structural shrinkage associated with the desaturation of the inter-aggregate pores (stage 2). During stage 2, macro-pores vacate, and their volume freezes. Fig. 8c shows that with further drying, aggregates may shrink while preserving the contact points, and the total sample volume decreases accordingly (i.e. nearly proportional shrinkage, stage 3). However, in peats, the volume change of the aggregates can be so large that the contact network becomes unstable. As a result, localised inter-aggregate collapse may occur, and aggregates rearrange in a new configuration, which reduces the macro porosity (Fig. 8d, stage 4). This mechanism can explain the reduction in total volume larger than the loss in water volume observed experimentally.

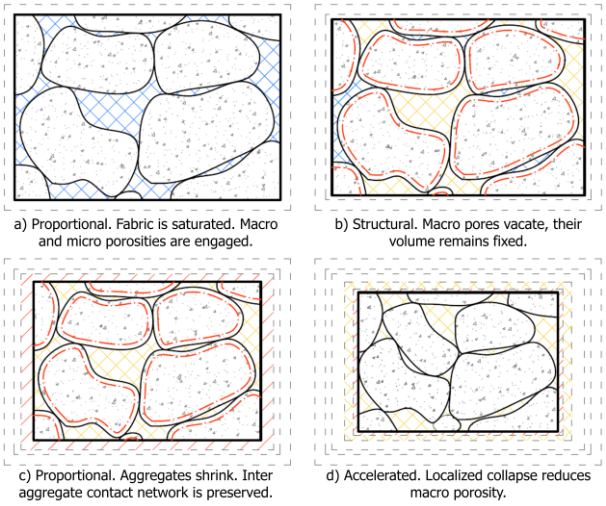

Fig. 8. Conceptual explanation of the accelerated shrinkage.

A simple and preliminary way of accounting for accelerated shrinkage is to allow the pores to shrink even after the air entry value is reached. To do so, the average skeleton stress used in the model is modified as in Equation 12.

$$\hat{p} = \begin{cases} s & \text{for } s \le \psi_{AE}(\phi) \\ \psi_{AE}(\phi) + \beta\left(s - \psi_{AE}(\phi)\right) & \text{for } s > \psi_{AE}(\phi) \end{cases} \qquad (12)$$

where β is an empirical coefficient, which scales down the suction effects after the air entry value. If the retention mechanism were purely capillarity, β would be equal to zero. The β coefficient is introduced as a preliminary way of accounting for the inter-aggregate collapse mechanism due to the shrinkage of the smaller pores. Fig. 9 shows the prediction of a simulation obtained using Distribution 2 with a β coefficient equal to 0.05.

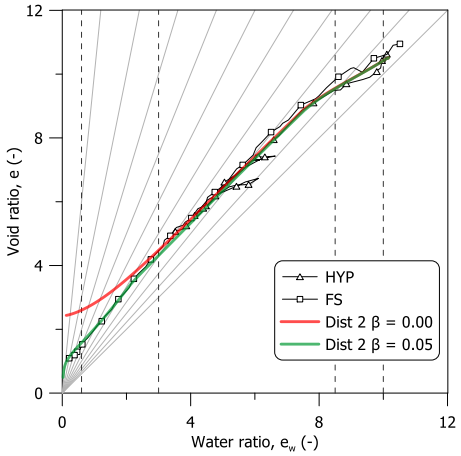

Fig. 9. Effects of the $\boldsymbol{\beta}$ coefficient.

By introducing the scaled suction after the air entry value in Equation 12, the acceleration of the shrinkage can be well captured. However, the linear scaling introduced by the β coefficient implies that the volume approaches zero at very large suctions, which does not match the experimental evidence.

5 Conclusions

The experimental evidence on drying-wetting cycles on natural fibrous peat suggests that it experiences distinct shrinkage stages during the drying process. Compared to mineral soils, these include a stage where the sample volume decreases more than the volume of water lost. The stage was observed on the tested peat between a water ratio of 3.0 and 0.6. Upon first drying, the volume change follows an almost linear relationship in the logarithmic space over a wide range of void ratios. The wetting and re-drying cycles exhibit a stiffer response similar to the over-consolidated behaviour expected upon unloading and reloading.

A laser distance sensor system was set up to track the shrinkage of peat samples, allowing for independent measurement of the radial, axial and volumetric strains. Measurements show that shrinkage is anisotropic at the start of drying and eventually converges towards an isotropic evolution at water ratios below 5.0.

The main features of shrinkage and water retention observed experimentally are qualitatively captured by a simple conceptual evolutionary capillary bundle approach. The simple model presented supports the physical interpretation of shrinkage modes as a consequence of the evolution of pore size distributions and interaction between pore size classes. Proportional, structural and residual shrinkage are naturally reproduced. Accelerated shrinkage is interpreted as a volumetric collapse of macro pore volume at a low water ratio. A preliminary approach to reproduce this stage has been implemented and shows good agreement with experimental data. However, additional work is needed to allow for the expected generation of macro porosity and other differential drying effects not included in the current formulation.

References

1. J. Xu, P. J. Morris, J. Liu, J. Holden, Catena (Amst), **160**, pp. 134–140, Jan. (2018), doi: 10.1016/J.CATENA.2017.09.010.
2. G. Kruse, E. D. Haan, *Characterisation and engineering properties of Dutch peats*, in Proceedings of the Second International Workshop on Characterisation and Engineering Properties of Natural Soils, (2006), doi: 10.1201/NOE0415426916.CH13.
3. A. M. Tang et al., Q. J. Eng. Geol. Hydrogeol., **51**, 2, pp. 156–168, (2018), doi: 10.1144/QJEGH2017-103.
4. H. Zhao, Can. Geotech. J., (2022), doi: 10.1139/CGJ-2021-0421.
5. G. Mesri, M. Ajlouni, J. Geotech Geoenviron **133**, 7, pp. 850–866, (2007), doi: 10.1061/(ASCE)1090-0241(2007)133:7(850).
6. ASTM, D5550-14 Standard Test Method for Specific Gravity of Soil Solids by Gas Pycnometer (2014).
7. ASTM, D2974-20e1 Standard Test Methods for Determining the Water (Moisture) Content, Ash Content, and Organic Material of Peat and Other Organic Soils (2020)
8. ASTM, D1997-20 Standard Test Method for Laboratory Determination of the Fiber Content of Peat and Organic Soils by Dry Mass (2020)
9. UMS, *Operation Manual HYPROP* Munich, Germany, (2015).
10. G. B. Stirk, Aust J Agric Res, **5**, 2, pp. 279–296, (1954), doi: 10.1071/AR9540279.
11. S. Gebhardt, H. Fleige, R. Horn, J Soils Sediments, **10**, 3, pp. 484–493, (2010), doi: 10.1007/S11368-009-0130-9/FIGURES/6.
12. R. Oleszczuk, K. Bohne, J. Szatylowicz, T. Brandyk, T. Gnatowski, J. Plant. Nutr. Soil Sci., **166**, 2, pp. 220–224, (2003), doi: 10.1002/JPLN.200390032.
13. R. Butterfield, Geotechnique, **29**, 4, pp. 469–480, (2015), doi: 10.1680/GEOT.1979.29.4.469.
14. E. J. den Haan, Geotechnique, **42**, 3, pp. 465–483, (2015), doi: 10.1680/GEOT.1992.42.3.465.
15. F. Cafaro, F. Cotecchia, *A structure-based approach to the estimate of the water retention curve of soils*, in 16th International Conference on Soil Mechanics and Geotechnical Engineering (Osaka), (2005), p. 483.
16. E. Romero, G. della Vecchia, C. Jommi, Geotechnique, **61**, 4, pp. 313–328, (2011), doi: 10.1680/GEOT.2011.61.4.313.
17. G. della Vecchia, C. Jommi, E. Romero, Int J Numer Anal Methods Geomech, **37**, 5, pp. 503–535, (2013), doi: 10.1002/NAG.1116.
18. G. della Vecchia, C. Jommi, E. Romero, *Hydro-mechanical coupling in unsaturated compacted clayey soils : modelling the water retention behaviour,* in 3rd International workshop of young doctors in geomechanics, (2008), pp. 21–24.
19. H. Yamaguchi, Y. Ohira, K. Kogure, Soils Found., **25**, 2, pp. 119–134, Jun. (1985), doi: 10.3208/SANDF1972.25.2_119.